Research Square

Preprints are preliminary reports that have not undergone peer review.
They should not be considered conclusive, used to inform clinical practice,
or referenced by the media as validated information.

Process Simulation and Comparative Performance Evaluation of SIFSIX-3- Cu and Mg-MOF-74 for Direct Air CO_2 Capture in Packed Bed Columns

Behrouz Bayati

b.bayati@ilam.ac.ir

Ilam University

Nima Rezaei

LUT University

Fatemeh Keshavarz

LUT University

Sohrab Zendehboudi

Memorial University

Bernardo Barbiellini

LUT University

Research Article

Keywords: SIFSIX-3-Cu, Direct air capture, Adsorption capacities, Desorption behavior, Packed bed modeling, Adsorption dynamics

Posted Date: August 6th, 2025

DOI: https://doi.org/10.21203/rs.3.rs-7213742/v1

License: This work is licensed under a Creative Commons Attribution 4.0 International License.
Read Full License

Additional Declarations: No competing interests reported.

Process Simulation and Comparative Performance Evaluation of SIFSIX-3-Cu and Mg-MOF-74 for Direct Air CO_2 Capture in Packed Bed Columns

Behrouz Bayati[1,2*], Nima Rezaei[3], Fatemeh Keshavarz[4], Sohrab Zendehboudi[2]*, Bernardo Barbiellini[3,5]

[1]Department of Chemical Engineering, Ilam University, Ilam, 6939177111 Iran

[2]Department of Process Engineering, Memorial University, St. John's, NL, A1C 5S7 Canada

[3]Department of Separation Science, School of Engineering Science, LUT University, FI-53850 Lappeenranta, Finland

[4]Department of Physics, School of Engineering Science, LUT University, FI-53850 Lappeenranta, Finland

[5]Department of Physics, Northeastern University, Boston, Massachusetts 02115, United States

[*]Email address of corresponding author: szendehboudi@mun.ca

[*]Email address of corresponding author: b.bayati@ilam.ac.ir

ABSTRACT

This study systematically evaluates the performance of SIFSIX-3-Cu in the direct air capture (DAC) process, with a comparison to Mg-MOF-74. The adsorption and working capacities of both sorbents are assessed, revealing that SIFSIX-3-Cu achieves substantial CO_2 adsorption even at low concentrations (400 ppm). Simulations of packed bed columns demonstrate that SIFSIX-3-Cu effectively captures CO_2 from ambient air, exhibiting a breakthrough time of 500 minutes, in contrast to only 70 minutes for Mg-MOF-74 at the same operating conditions. Temporal assessments of CO_2 uptake along the column indicate that SIFSIX-3-Cu attains a CO_2 uptake of 1.4 mmol g^{-1} under ambient conditions, while Mg-MOF-74 reaches only 0.12 mmol g^{-1}. The enhanced performance of SIFSIX-3-Cu is attributed to its superior affinity for CO_2 at the atmospheric concentration. In addition, the desorption behaviors of both materials are investigated. SIFSIX-3-Cu releases CO_2 gradually because of its smaller pore opening and stronger interactions with CO_2 whereas Mg-MOF-74 displays a two-step desorption mechanism. Furthermore, notable differences are observed in the temperature profiles during the adsorption and desorption stages. SIFSIX-3-Cu requires higher temperatures and lower pressures for efficient CO_2 desorption, while the larger pore dimensions of Mg-MOF-74 facilitate the CO_2 release. Overall, SIFSIX-3-Cu demonstrates significant promises for DAC applications, particularly due to its superior CO_2 adsorption capacity at low concentrations, highlighting its potential for effective CO_2 capture from ambient air.

Key words: SIFSIX-3-Cu; Direct air capture; Adsorption capacities; Desorption behavior; Packed bed modeling; Adsorption dynamics

1. INTRODUCTION

Direct air capture (DAC) has emerged as a critical technology in the global effort to mitigate climate change by reducing atmospheric carbon dioxide (CO_2) levels [1][2]. This process commonly involves CO_2 capture using sorbents or solvents, followed by its storage for long-term sequestration [3]. Despite companies and research institutions working on developing DAC technologies and scaling them up for commercial use, the technology is still in its early stages and faces several challenges such as high costs, energy requirements, and scalability [4]. The advancements of materials science and engineering have led to significant improvements in the efficiency of DAC, enhancing its viability for climate change mitigation. This has motivated companies and research groups to actively develop and improve efficient and cost-effective DAC methods [5][6], including solid sorbents (e.g., zeolites, metal-organic frameworks (MOFs), or activated carbon), and liquid sorbents (e.g., aqueous amines, amino acids, or ionic liquids).

The efficiency of most DAC technologies is limited by the low concentration of CO_2 in the atmosphere. Some chemical methods using, for instance, amines and alkaline solutions can absorb CO_2 from the air even at low CO_2 concentrations; however, the regeneration stage is energy-intensive and costly [7]. Therefore, solid adsorbents are suggested for DAC because of their lower energy demand, lower operational costs, easier regeneration, minimal infrastructure requirement, and scalability potential [8]. Still, the choice of the proper solid adsorbent with strong CO_2 adsorption capacity is crucial to ensure its efficiency for selective CO_2 removal [9][10][11] and adsorbent regeneration through a combination of heat and vacuum [12]. If an appropriate adsorbent is chosen, temperature swing adsorption (TSA) technologies can offer significant cost reduction for carbon capture [13]. Therefore, the adsorbent plays a central role in efficient grid-scale DAC. The ideal adsorbent should efficiently capture CO_2, exhibit fast kinetics, high selectivity, and remarkable physical and chemical stability, in addition to providing strong CO_2 adsorption [14]. Metal-organic frameworks (MOFs) have emerged as promising adsorbent candidates due to their highly porous crystalline structures, which are constructed through the bonding of metal ions and organic ligands. When incorporated with pre-functionalized ligands, MOFs' modular and hybrid properties allow for precise adjustment of CO_2 affinity, presenting effective solutions for a range of carbon capture challenges [15][16]. In particular, Mg-MOF-74, UiO-66-NH_2, and HKUST-1 have demonstrated efficient CO_2 capture capabilities [17][18]. Among these, Mg-MOF-74 has been widely studied for its high CO_2 uptake and selectivity, making it a benchmark material for carbon capture applications. However, the search for more efficient adsorbents continues, driven by the need for materials that can operate effectively under ambient conditions with minimal energy input. Recently, a new class of materials known as hybrid ultra-microporous materials (HUMs) has shown exceptional promise for CO_2 capture. These materials feature extremely small pore sizes and strong electrostatic interactions, enabling them to tightly encapsulate CO_2 while maintaining high selectivity against other atmospheric components, such as N_2 [19]. These crystalline frameworks are composed of square [M(pyrazine)2^{2+}]n grids linked by counter anions, which act as pillars. Among HUMs, SIFSIX-3-X (where X = Ni, Cu, or Zn) has garnered

significant attention due to its robust interaction with CO_2, attributed to its unique structural properties. Among HUMs, SIFSIX-3-Cu has garnered significant attention due to its robust CO_2 affinity even at extremely low concentrations (~400 ppm), stability in humid environments, and potential for scalable deployment [15]. The potential application of SIFSIX-3-Cu has been explored in several studies. For instance, Shekhah et al. [20] and Forest et al. [21] investigated its adsorption properties, while our previous study utilized molecular dynamics (MD), grand canonical Monte Carlo (GCMC) simulations, and density functional theory (DFT) calculations to examine CO_2 and H_2O adsorption behaviors [22]. These studies confirmed the material's high CO_2 uptake capacity but also revealed the negative impact of humidity on its performance, underscoring the need for moisture removal prior to the DAC process.

Despite these advancements, a significant research gap remains in understanding the performance of SIFSIX-3-Cu under realistic operational conditions, particularly in packed bed configurations for grid-scale DAC applications. While molecular-level insights into SIFSIX-3-Cu's adsorption behavior have been well-documented, there is a lack of comprehensive studies evaluating its performance in continuous adsorption/desorption cycles and comparing it to established materials like Mg-MOF-74, a well-established material for carbon capture. This gap hinders the practical implementation of SIFSIX-3-Cu in large-scale DAC systems, where factors such as adsorption kinetics, diffusion behavior, and desorption efficiency play critical roles. To address this gap, this study investigates the performance of SIFSIX-3-Cu in packed bed columns and compares it to Mg-MOF-74, a well-established carbon capture material. The adsorption and diffusion behaviors of both N_2 and CO_2 in SIFSIX-3-Cu are examined in detail, and the process conditions for adsorption and desorption are systematically analyzed. By extending the molecular-level insights from our earlier work to operational conditions, this study aims to provide a comprehensive evaluation of SIFSIX-3-Cu's potential as an advanced sorbent for DAC applications.

2. MATERIALS AND METHODS

In this work, a dynamic model is employed to simulate a continuous adsorption/desorption cyclic process using SIFSIX-3-Cu and Mg-MOF-74 as sorbents for DAC within a single packed bed column. The inner diameter and length of the column are set to d = 0.005 m and L = 0.027 m, respectively. The CO_2 concentration in the feed is maintained at 400 ppm, while the temperature and pressure are kept at ambient conditions. The accurate determination of adsorption and diffusion parameters is crucial for modeling packed bed systems. These parameters are typically obtained by conducting adsorption isotherms at various temperatures, which helps establish optimal adsorption and desorption conditions. In this study, the Grand Canonical Monte Carlo (GCMC) method is used to compute the adsorption isotherms for SIFSIX-3-Cu. Additionally, kinetic models are applied to derive kinetic parameters, such as the diffusion coefficient. For Mg-MOF-74, the required parameters are obtained from previously documented literature and incorporated into the modeling process[12][23].

2.1 Grand Canonical Monte Carlo (GCMC) Simulations

The adsorption isotherms and isosteric heats of pure N_2 and CO_2 adsorption into SIFSIX-3-Cu are calculated at 298, 323, 373, 398 and 423 K and pressures up to 1 bar using GCMC simulations. The simulations are performed through the sorption module of the Materials Studio software. To accommodate enough adsorbent molecules into the structure and enhance the precision of the simulations, the unit cell of SIFSIX-3-Cu [20][24][25] is extended and a 3 × 3 × 4 supercell is created (see Fig. 1). The MOF's framework is assumed rigid, and periodic boundary conditions are applied in all dimensions. The adsorbate/SIFSIX-3-Cu interactions are computed as the atom-based summation of van der Waals and electrostatic interactions using the cutoff radius of 12.5 Å [22]. The van der Waals interactions are computed using the Lennard Jones (LJ) parameters adopted from the Universal Force Field (UFF). Although some studies suggest that UFF overestimates gas adsorption isotherms of MOFs[26], our earlier study [22] revealed that UFF outperforms the Dreiding, UFF_mod_C_2H_2-CO_2 and Polymer Consistent Force Field (PCFF) forcefields and reproduces the experimental isotherms of N_2 and CO_2 adsorption into SIFSIX-3-Cu, accurately. The electrostatic interactions are calculated using the Ewald summation method with 0.001 kcal/mol accuracy. At each temperature and pressure, 1×10^6 simulation steps are conducted to guarantee equilibration.

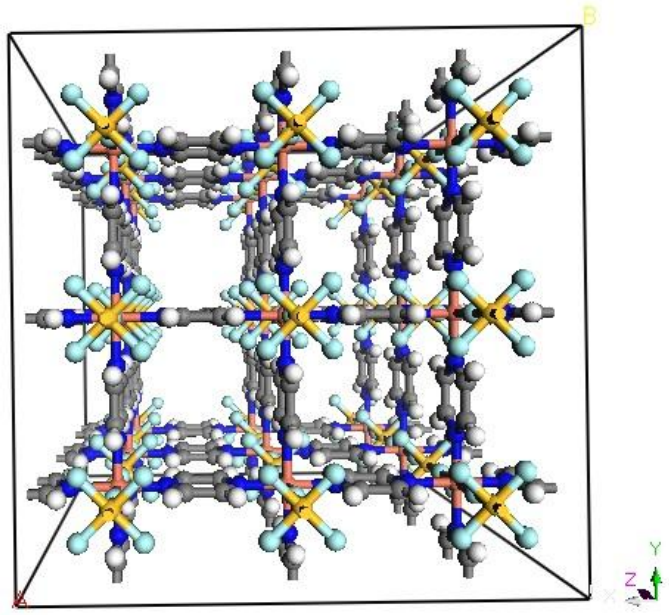


Figure 1. Schematic view of the 3 × 3 × 4 SIFSIX-3-Cu supercell[25];

Si ●, N ●, F ●, C ●, Cu ●, H ○

2.2 Modeling of Packed Bed Adsorption Column

The modeling of adsorption and desorption within a cylindrical packed bed column is founded on the conservation laws of momentum, energy, and mass. Some key assumptions are incorporated into the model: (i) ideal gas behavior, (ii) application of the linear driving force (LDF) model, (iii) a constant column porosity, (iv) one-dimensional (axial) dispersion, (v) thermal equilibrium between the column (initially saturated with N_2) and the feed stream, and (vi) utilization of the Ergun equation for calculating the pressure drop across the fixed bed column[23].

The concentration profiles of the gas phase are characterized using the continuity equation, given below.

$$-\varepsilon_b D_{ax}\frac{\partial^2 c_i}{\partial z^2}+\frac{\partial}{\partial z}(u_g c_i)+\varepsilon_t\frac{\partial c_i}{\partial t}+\rho_b\frac{\partial q_i}{\partial t}=0 \tag{1}$$

where c_i stands for the concentration of component i in the gas phase, u_g is superficial gas velocity, ρ_b is adsorbent bulk density, D_{ax} refers to the axial dispersion coefficient along the bed, ε_b is the interparticle voidage, ε_t is total bed voidage, and q_i introduces the average amount of adsorbed species i [27][28]. The first term represents axial dispersion, while the subsequent term pertains to convection. The third and fourth terms of the equation correspond to gas phase accumulation and mass transfer kinetics (adsorption rate), respectively. The model is developed based on the following initial and boundary conditions:

$$c(t=0,z)=0 \tag{2}$$

$$c(t,z=0)=0 \tag{3}$$

$$\left.\frac{\partial c}{\partial z}\right|_{(t,z=L)}=0 \tag{4}$$

2.2.1 Isotherm model

The single-site (Eq. 5) and dual-site (Eq. 6) Langmuir models are applied to analyze the N_2 and CO_2 adsorption isotherms obtained from the GCMC simulations[29].

$$\frac{q_e}{q_s} = \frac{bP}{1+bP} \tag{5}$$

$$q_e = \frac{q_{s1} b_1 P}{1+b_1 P} + \frac{q_{s2} b_2 P}{1+b_2 P} \tag{6}$$

In the above equations, b is the adsorption constant of the single-site model, q_s denotes the maximum adsorption value, P is the pressure, q_e stands for the the adsorption equilibrium amount, b_1 and b_2 represent the Langmuir adsorption parameters of adsorption site in the dual-site model, and q_{s1} and q_{s2} represent the maximum adsorption capacities at adsorption sites 1 and 2, respectively[29]. The temperature dependency of b_1 and b_2 is described using the Arrhenius equation:

$$b_i = b_{0i} e^{-E/RT} \tag{7}$$

where b_{0i} is a constant factor, E symbolizes the activation energy, T is the temperature, and R is the universal gas constant.

2.2.2 Mass transfer kinetics

The mass transfer kinetics is modeled using the LDF model:

$$\left(\frac{\partial q_i}{\partial t}\right) = k_i (q_{ei} - q_i) \tag{8}$$

where q_{ei} is the average equilibrium amount of adsorbed component i at partial pressure p_i, and q_i introduces the average amount of component i, both averaged over an adsorbent particle[30]. The parameter k_i is the mass transfer coefficient and is estimated from the film, macroporous, microporous resistances of the gases in the porous adsorbent as[31]:

$$\frac{1}{k_i} = \frac{r_p q_i}{3 k_{f,i} c_i} + \frac{r_p^2 q_i}{15 \varepsilon_p D_{pi} c_i} + \frac{r_c^2}{15 D_{ci}} \tag{9}$$

where c_i and q_i are respectively the adsorbate's concentrations at the gas and solid phases, ε_p refers to the particle porosity, r_p is the radius of the adsorbent particle, and r_c denotes the

adsorbent's crystal radius. $D_{p,i}$, $k_{f,i}$, and $D_{c,i}$ are the macroporous diffusion coefficient, film mass transfer coefficient, and microporous diffusion coefficient, respectively[31]. The first term on the right-hand side of Eq. (9) accounts for the gas film resistance. The second term in the equation represents macroporous resistance, while the last term accounts for microporous resistance to gas diffusion. Since SIFSIX-3-Cu does not undergo shaping, the dominant resistance term is assumed to be intraparticle diffusion, which refers to the diffusion of molecules into the microporous solid. Therefore, we simplify the mass transfer coefficient equation to the following form:

$$\frac{1}{k_i} = \frac{r_p^2}{15 D_{ci}} \tag{10}$$

The diffusion in the microporous solid is considered as the rate-controlling step for mass transfer into the particle. It is estimated by the following equation[32][33][34]:

$$\frac{\partial q_i}{\partial t} = \frac{D_{c,i}}{r^2} \frac{\partial}{\partial r} \left(r^2 \frac{\partial q_i}{\partial r} \right) \tag{11}$$

where q_i *is* the adsorption amount of component i, $D_{c,i}$ represents the diffusion coefficient inside the solid micropores, and r *is the* radial position. To solve Eq. (11) analytically, we assume a constant concentration on the external surface of the solid, leading to the formulation of Eq. (12) as follows [32]:

$$\frac{q_i}{q_{ei}} = 1 - \frac{6}{\pi^2} \sum_{n=1}^{\infty} \frac{1}{n^2} \exp\left(\frac{-D_{c,i} n^2 \pi^2 t}{r_c^2} \right) \tag{12}$$

where q_i is the average loading of species i at time t, q_{ei} is the average amount of species i in the solid phase at equilibrium, and r_c denotes the radius of particle.

For long-time diffusion ($\frac{q_i}{q_{ei}} > 0.7$), Eq.(12) can be re-written as[32][35].

$$\frac{q_i}{q_{ei}} = 1 - \frac{6}{\pi^2}\exp\left(\frac{-D_{c,i}\pi^2 t}{r_c^{\,2}}\right) \tag{13}$$

$$\ln(1 - \frac{q_i}{q_{ei}}) = \ln\frac{6}{\pi^2} - \frac{D_{c,i}\pi^2 t}{r_c^2} \tag{14}$$

From which, $D_{c,i}$ can be estimated by plotting $\ln(1 - {}^{q_i}/_{q_{ei}})$ vs. t.

2.2.3 Energy balance

Non-isothermal energy balance with no solid conduction is employed for vacuum temp swing adsorption (VTSA) process simulation. The energy balance equations for the gas and solid phase are presented as follow[36][37][27]:

$$-k_{ga}\varepsilon_b\frac{\partial^2 T_g}{\partial z^2} + C_{vg}u_g\rho_g\frac{\partial T_g}{\partial z} + \varepsilon_t C_{vg}\rho_g\frac{\partial T_g}{\partial t} + P\frac{\partial u_g}{\partial z} + h_{gs}a_p(T_g - T_s) + \frac{4h_w}{d_b}(T_g - T_w) = 0 \tag{15}$$

$$-k_{sa}\frac{\partial^2 T_s}{\partial z^2} + C_{ps}\rho_s\frac{\partial T_s}{\partial z} + \rho_s\sum_{i=1}^{n}(C_{pai}q_i)\frac{\partial T_s}{\partial t} + \rho_s\sum_{i=1}^{n}(\Delta H_i\frac{\partial q_i}{\partial t}) - h_{gs}a_p(T_g - T_s) = 0 \tag{16}$$

Here, k_{ga} and k_{sa} are respectively the thermal conductivities of the gas phase and the adsorbent particle, C_{vg} introduces the constant volume heat capacity of the gas phase, C_{ps} represents the specific heat capacity of the adsorbent, h_{gs} and h_w are the gas–solid and gas-wall heat transfer coefficients, ρ_g is gas density, ρ_s is adsorbent density, ε_b is bed porosity, ε_t is overall porosity, a_p is particle specific superficial area, q_i is the amount of adsorbed component i, ΔH_i is the heat of adsorption for component i, and T_g and T_s stand for respectively the gas and solid phase temperatures in K.

2.2.4 Momentum balance

Pressure drop along the length of column is calculated using the Ergun model [38]:

$$\frac{\partial P}{\partial z} = -\left(\frac{1.5\times10^{-3}(1-\varepsilon_b)^2}{(2r_p\psi)^2}\mu_g u_g + 1.75\times10^{-5} M\rho_g \frac{(1-\varepsilon_b)}{2r_p\psi\varepsilon_b{}^3} u_g^2 \right) \quad (17)$$

where μ_g is the gas dynamic viscosity, ρ_g indicates the gas density, r_p refers to the particle's radius adsorbent pellet, ψ is the adsorbent's pellet shape factor, M is the molecular weight of the gas, and u_g represents the superficial gas velocity.

2.3 Methodology Flowchart

The methodology of this study is systematically illustrated in figure 2, which outlines the key steps involved in evaluating the performance of SIFSIX-3-Cu and Mg-MOF-74 for DAC. The process begins with defining the system parameters, including column dimensions and feed conditions. Next, adsorption isotherms are conducted using GCMC simulations for SIFSIX-3-Cu, while the Linear Driving Force LDF model are applied to MTC. The Ergun equation for pressure drop calculations. The adsorption process is simulated to analyze breakthrough curves and temporal CO_2 uptake, followed by desorption simulations to evaluate CO_2 release efficiency under varying temperatures and pressures. The performance of SIFSIX-3-Cu is compared to Mg-MOF-74 in terms of breakthrough time, CO_2 uptake capacity, and desorption efficiency.

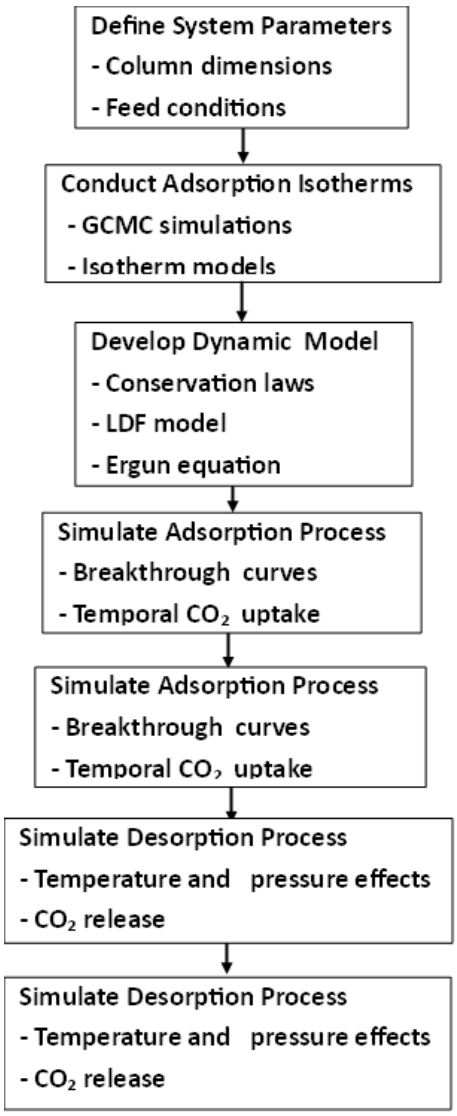


Fig. 2. Flowchart of the methodology for evaluating materials in direct air capture

2.4 Limitations and drawbacks

Although MOFs exhibit promising performance for CO_2 capture under dry conditions, their adsorption capacity and selectivity can be significantly reduced in the presence of water vapor. This limitation arises due to the hydrophilic nature of the open metal sites in these MOFs, which tend to preferentially adsorb water molecules over CO_2, thereby occupying the active sites and decreasing overall efficiency. In practical applications such as DAC, where ambient air contains considerable humidity, this drawback must be addressed to maintain the adsorbent's performance. Therefore, prior to the CO_2 separation stage, it is essential to incorporate a pre-treatment step for moisture removal using conventional and cost-effective drying methods (e.g., desiccant beds, refrigeration dryers). This preliminary dehydration ensures that the main adsorption column operates under near-dry conditions, preserving the CO_2 capture efficiency of the selected MOFs.

As such, while the current process model assumes dry feed conditions, this simplification remains valid and practically achievable.

3. RESULTS AND DISCUSSION

3.1 GCMC

Since desorption of the gases adsorbed during DAC occurs at higher than adsorption temperatures, the adsorption isotherms of CO_2 and N_2 are calculated at several temperatures using GCMC simulations. First, the method's validity is assessed by comparing the GCMC results at 298 K with the data reported by Adil et al. [39] and Yuan et al.[40] . The agreement observed in Fig. S1 (in Supporting Information) declares the accuracy of the molecular simulation approach for studying gas adsorption by SIFSIX-3-Cu. Subsequently, the isotherms of CO_2 and N_2 are further examined at different temperatures. The outcomes depicted in Fig. 2 demonstrate a CO_2 uptake of 1.45 mmol g^{-1} by SIFSIX-3-Cu at 0.0004 kPa and 298 K, highlighting the SIFSIX-3-Cu remarkable affinity for CO_2 even at low concentrations and ambient temperatures. Also, the findings reveal significantly reduced gas adsorption levels at temperatures exceeding 373 K. As a result, it is recommended that the desorption process should be conducted at temperatures above 373 K to ensure optimal efficiency. By observing Fig. 3 and 4, it becomes evident that the isotherm data at different temperatures align well with the single-site Langmuir model. This model effectively describes the uptake behaviors of CO_2 and N_2, offering a comprehensive understanding of the adsorption process for these gases. It should be noted that the maximum adsorption capacities of CO_2 (2.7 mmol/g) and N_2 (2.3 mmol/g) on SIFSIX-3-Cu are relatively close. Therefore, the extended Langmuir model, which assumes equal or similar saturation capacities across components, can be appropriately applied to describe the binary adsorption behavior. Additionally, in the absence of large deviations in saturation capacities, the extended Langmuir model is known to provide a sufficiently accurate estimation of competitive adsorption for binary gas mixtures, particularly when validated against reliable single-component isotherms. Given the good agreement between GCMC results and the fitted Langmuir isotherms across all temperatures (Figs. 3 and 4), and the comparable q_sat values for the two gases, the use of the extended Langmuir model is both practical and justified. Otherwise, if the saturation capacities of CO_2 and N_2 were significantly different, the use of thermodynamically consistent models such as IAST (Ideal

Adsorbed Solution Theory) would have been necessary to accurately capture the competitive adsorption behavior.

The extended Langmuir model is used for predicting the equilibrium values of adsorbed CO_2 and N_2 amounts from their gas mixtures [41]:

$$q_{ei} = \frac{b_{1i} e^{b_{2i}/T} p_i}{1 + \sum b_{3i} e^{b_{4i}/T} p_i} \tag{18}$$

Here, q_{ei} (kmol kg^{-1}) is the adsorbed amount, p_i is the equilibrium pressure (bar), T stands for the temperature (K), and the units of the isotherm parameters include b_{1i} = kmol kg^{-1} bar^{-1}; $b_{2i} = b_{4i}$=K; and b_{3i} = bar^{-1}. The estimated Extended Langmuir parameters for CO_2 and N_2 adsorption onto SIFSIX-3-Cu are listed in Table 1.

Table 1. Extended Langmuir model adsorption parameters for CO_2 and N_2 on SIFSIX-3-Cu

component	b_1 (kmol kg^{-1} bar^{-1})	b_2 (K)	b_3 (bar^{-1})	b_4 (K)
CO_2	4.19×10^{-9}	6339	1.54×10^{-3}	6339
N_2	4.83×10^{-7}	1870	1.61×10^{-4}	1670

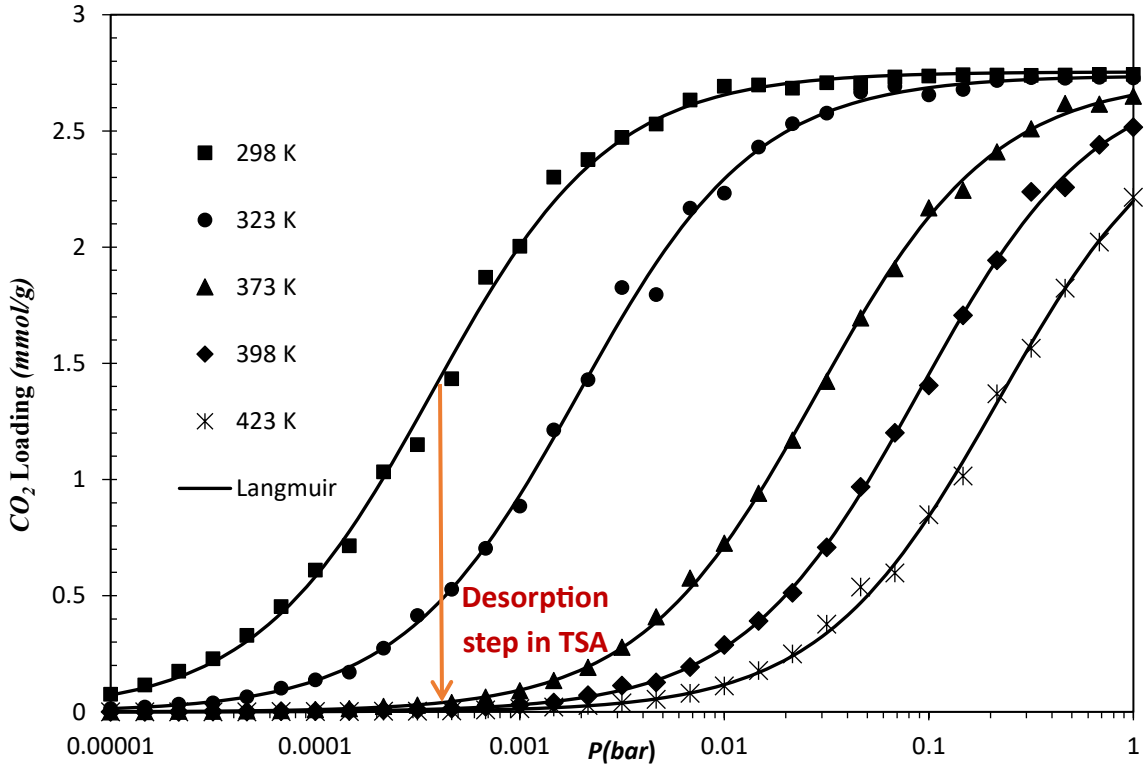


Figure 3. Langmuir adsorption isotherms from GCMC for pure CO_2 and SIFSIX-3-Cu at different temperatures and pressure range up to 1 bar

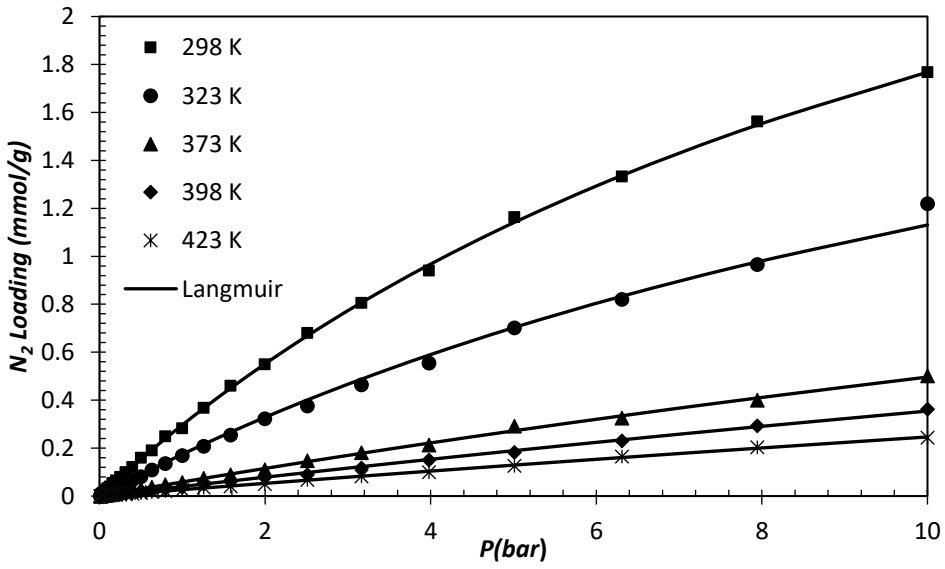


Figure 4. Langmuir adsorption isotherms from GCMC for pure N_2 and SIFSIX-3-Cu at different temperatures and pressure range up to 10 bar

Because of lack of experimental data for the adsorption isotherms for CO_2 and N_2 on SIFSIX-3-Cu at different temperatures, we use GCMC simulation to calculate the adsorption isotherms at different temperature and pressure levels. For MOF-74, experimental data are available for the adsorption and diffusion of CO_2 and N_2, that are utilized for modeling purposes.

The equilibrium adsorbed amount q_i for CO_2 and N_2 mixture on Mg-MOF-74 is calculated from the dual-site Langmuir-2 model [42]:

$$q_i = \frac{(b_{1i} + b_{2i}T)b_{3i}e^{b_{4i}/T}p_i}{1+\sum b_{3i}e^{b_{4i}/T}p_k} + \frac{(b_{5i} + b_{6i}T)b_{7i}e^{b_{8i}/T}p_i}{1+\sum b_{7i}e^{b_{8i}/T}p_k} \quad (19)$$

where q_{ei} represents the equilibrium loading of component i in adsorbent, kmol·kg^{-1}, p_i is is the partial pressure of component i, bar, T is the adsorbent temperature, K, and bi is the isotherm parameters. The units of b_{1i} and b_{5i} are kmol·kg^{-1}, the units of b_{2i}, b_{4i}, b_{6i} and b_{8i} are K, and the units of b_{3i} and b_{7i} are bar^{-1}.

3.2 Mass Transfer Coefficient

The mass transfer coefficient holds significant importance within the context of the adsorption process, as it serves as an indicator for the rate at which molecules are transferred from the gaseous phase to the adsorption sites present on the solid adsorbent. Zeolite and MOF powders are typically shaped into spherical or cylindrical beads (see Fig. 5). The beads contain macropores, mesopores and micropores. The micropores are the inherent pores of zeolites and MOFs.

The existing literature data on the adsorption of CO_2 and N_2 on SIFSIX-3-Cu utilized a powder adsorbent, which implies that the adsorption mechanism did not involve the participation of macroporous structures. Furthermore, given the small size of the micropores in SIFSIX-3-Cu, the primary hindrance to mass transfer is attributed to the transfer occurring within the microporous. No data has been reported for mass transfer coefficient of CO_2 and N_2 on SIFSIX-3-Cu in literatures. Therefore, in this research, the mass transfer coefficient is determined by fitting the adsorption data against time, as reported by Shikhah et al. [20], using Eq. (14). The fitting curves, shown in Figures S2 and S3, demonstrate a good agreement with Eq. (14). The calculated MTC for CO_2 and N_2 are found to be 0.0006 and 0.00045 1/s, respectively.

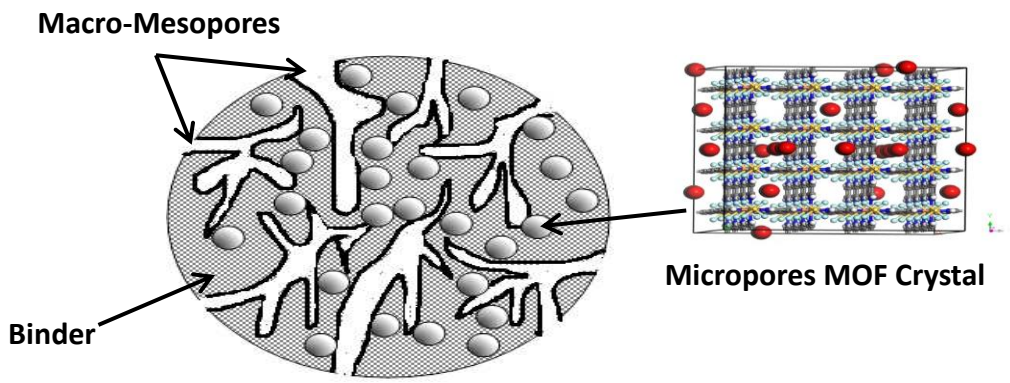


Figure 5. Structure of a bonded MOF bead showcasing macro-, meso-, and micropores [43].

3.3 Packed Bed Model Results

3.3.1 Model validation

To assess the validity of the proposed model, a comparison is made between the model-predicted breakthrough curve and the results reported by Qasem and Ben-Mansour et al. [12][23] for CO_2 capture using MOF-74, as shown in Figure 6. The validation process involves using the same adsorption isotherms, kinetic coefficients, dimensions of the adsorption column, and operating conditions as those described by Ben-Mansour et al. [23]. The results reveal a satisfactory correlation between the model predictions and the findings reported by Ben-Mansour et al. [23] Specifically, the shape of the breakthrough curve and the breakthrough time are effectively replicated, demonstrating that the model accurately reflects the adsorption behavior of the sorbent within the packed bed. This further substantiates the accuracy and reliability of the mathematical model employed.

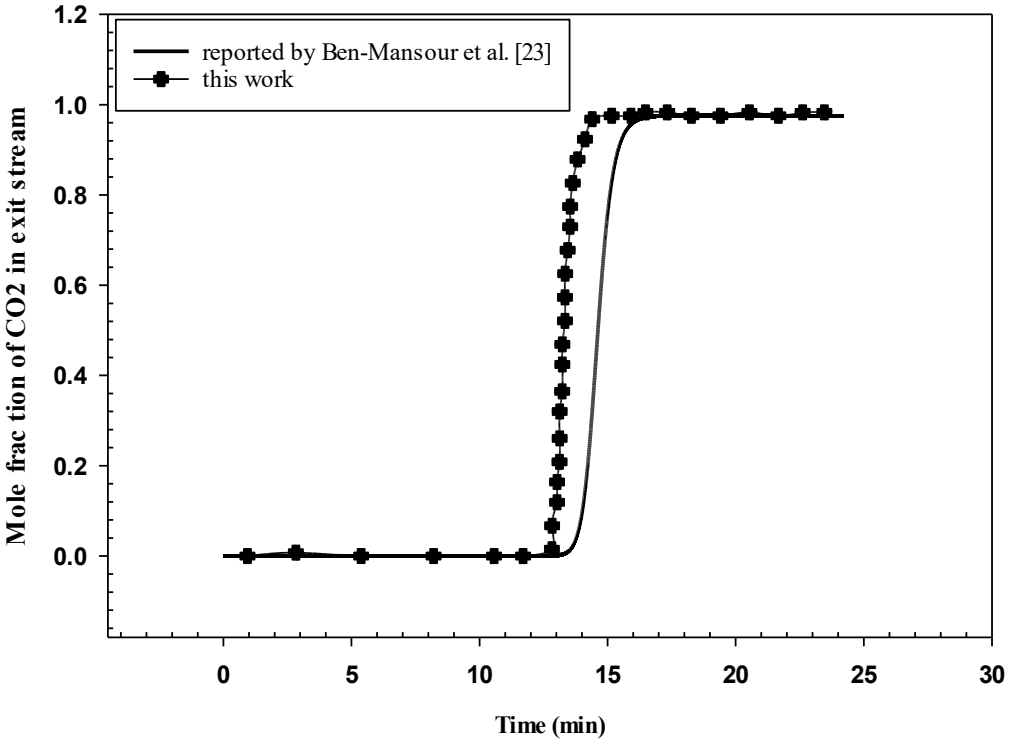


Figure 6. Comparison of model validation breakthrough curves for CO_2 adsorption on Mg-MOF-74 at 298 K with a CO_2:N_2 molar ratio of 15:85. The solid line represents the experimental data reported by Ben-Mansour et al.[23], while the symbols represent the results from the proposed model.

3.3.2 Adsorption breakthrough curves

Fig. 7 shows CO_2 mole fraction evolution along the packed bed column with a column height of L and at five various elevations at 0.2 L, 0.4 L, 0.6 L, 0.8 L, and L from the bed inlet side . All the process condition are same for both SIFSIX-3-Cu and Mg-MOF-74 packed beds. All model conditions are summarized in Tables S1 and S2. The CO_2 concentration in the feed is 400 ppm, temperature and pressure are 298 K and 1.25 bar, respectively. Fig. 6 shows that the CO_2 mole fraction in the outlet stream of SIFSIX-3-Cu packed bed reaches 0.0004 (similar to the inlet concentration) after a 500 min, while the breakthrough curve is 60-70 min for Mg-MOF-74 (see Fig. 8). This comparison shows that the potential of SIFSIX-3-Cu for the DAC process is much

higher than MOF, which is due to the high tendency of SIFSIX-3-Cu to adsorb CO_2 even at low concentrations[22].

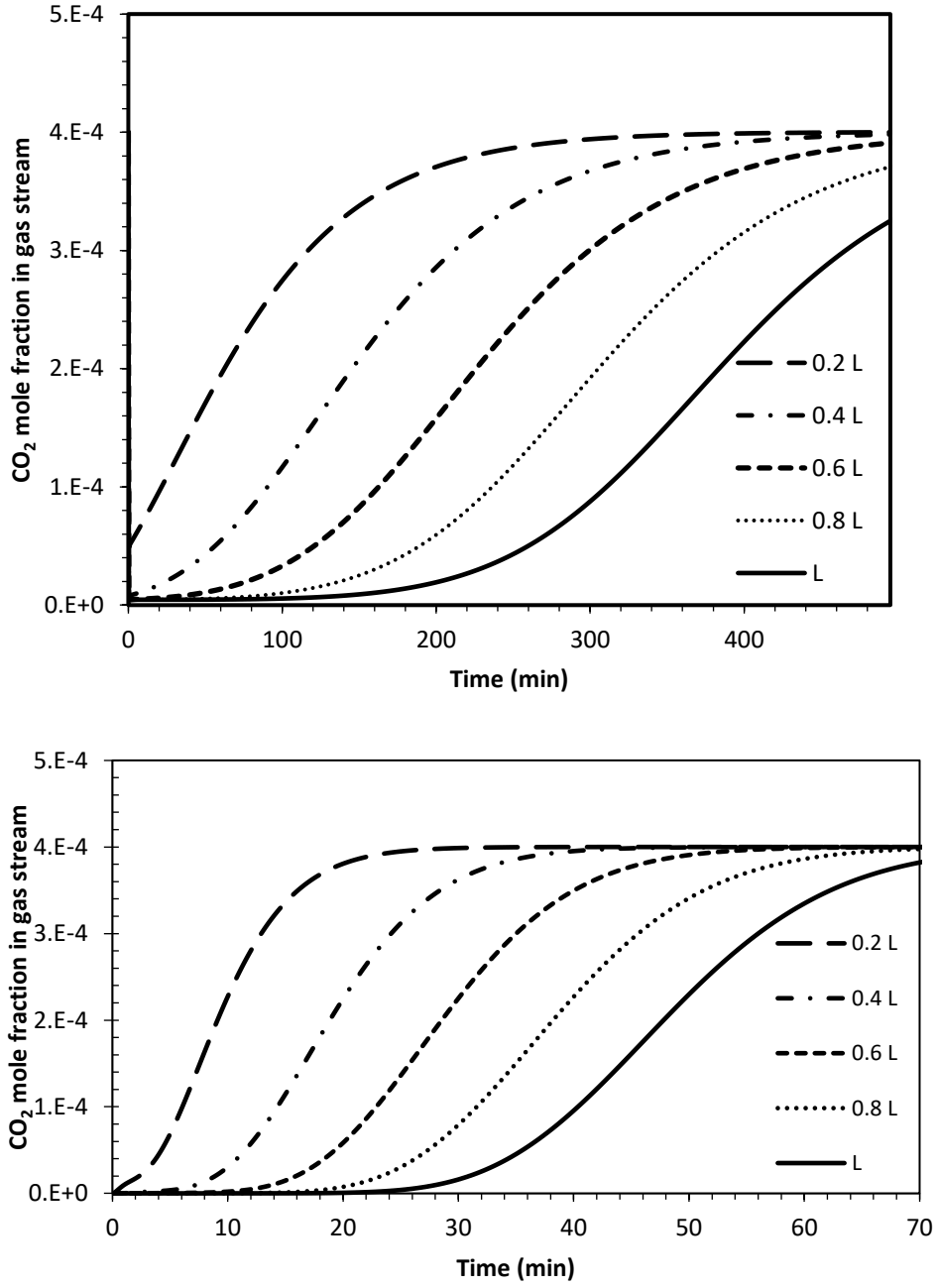
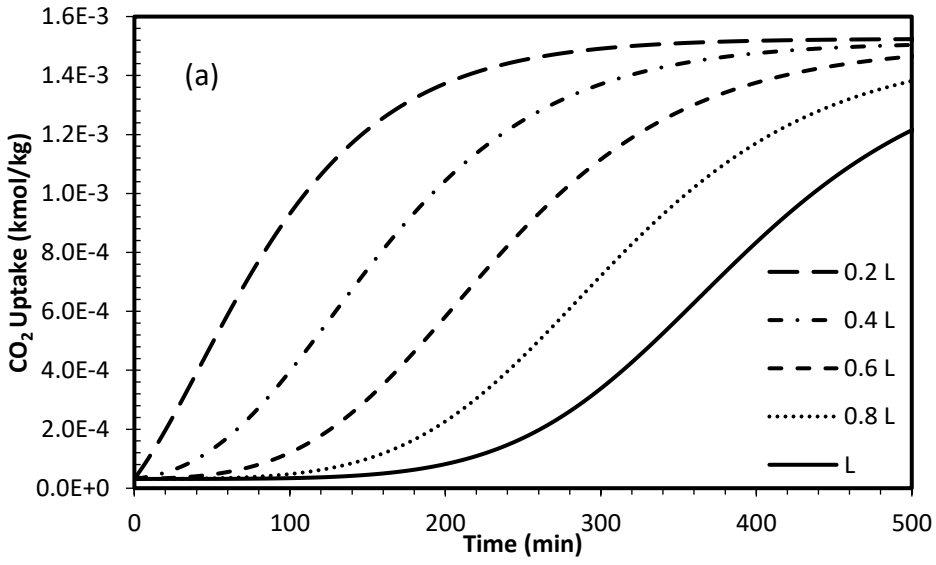


Figure 7. Breakthrough curves of CO_2 adsorption on (a) SIFSIX-3-Cu and (b) Mg-MOF-74 at various locations along the bed, with a CO_2 concentration of 400 ppm in N_2, operating conditions of 1.25 bar, 298 K, and a feed flow rate of 20 mL min^{-1}.

For a more detailed analysis, Fig.8 presents the temporal variation of CO_2 uptake in different layers of the column. It is evident that SIFSIX-3-Cu exhibits a maximum CO_2 uptake of approximately 1.4 mmol/g under the ambient conditions with a CO_2 concentration of 400 ppm. In contrast, Mg-MOF-74 achieves a maximum CO_2 uptake of around 0.12 mmol g^{-1}. This stark contrast highlights the superior performance and higher potential of SIFSIX-3-Cu in the DAC process compared to Mg-MOF-74. Although the maximum CO_2 uptake capacity of SIFSIX-3-Cu (2.5 mmol g^{-1}) is lower than that of Mg-MOF-74 (8 mmol g^{-1}) at high CO_2 concentrations, SIFSIX-3-Cu demonstrates superior performance at low CO_2 concentrations, which are representative of direct air capture conditions. Interestingly, the isotherm curves (See Fig. 3) reveal that SIFSIX-3-Cu reaches its maximum CO_2 uptake at pressures below 0.01 kPa. Moreover, the CO_2 uptake on SIFSIX-3-Cu at a pressure of 0.0004 kPa (equivalent to a concentration of 400 ppm) amounts to 1.45 mmol g^{-1}. Conversely, even at 0.034 kPa, the CO_2 uptake for Mg-MOF-74 is only 0.01 mmol g^{-1} [44][45]. The remarkable capacity of SIFSIX-3-Cu for CO_2 adsorption (even at low concentrations) is vital considering that the CO_2 concentration in the DAC process is typically around 400 ppm (with a partial pressure of CO_2 equivalent to 0. 0004 kPa). This attribute renders it notably suitable for the DAC process.



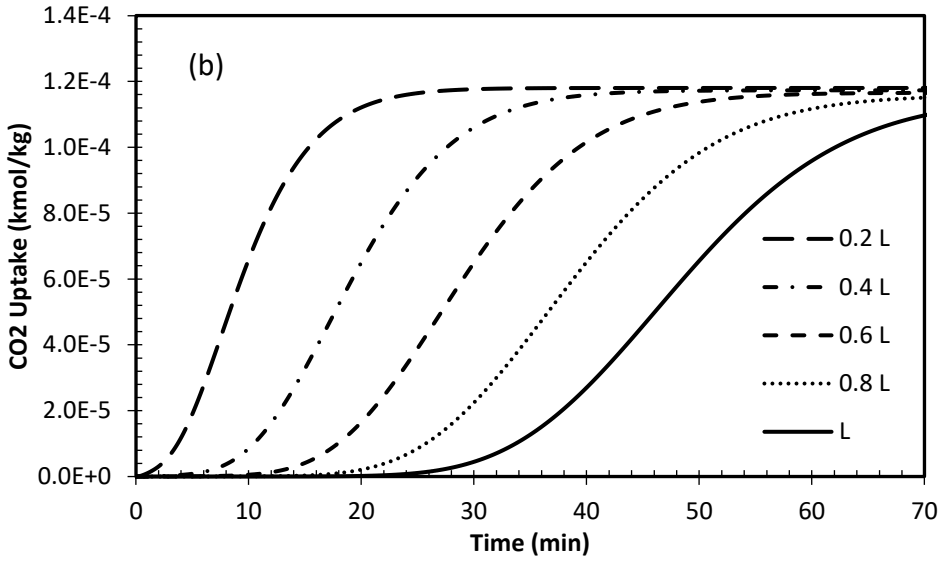
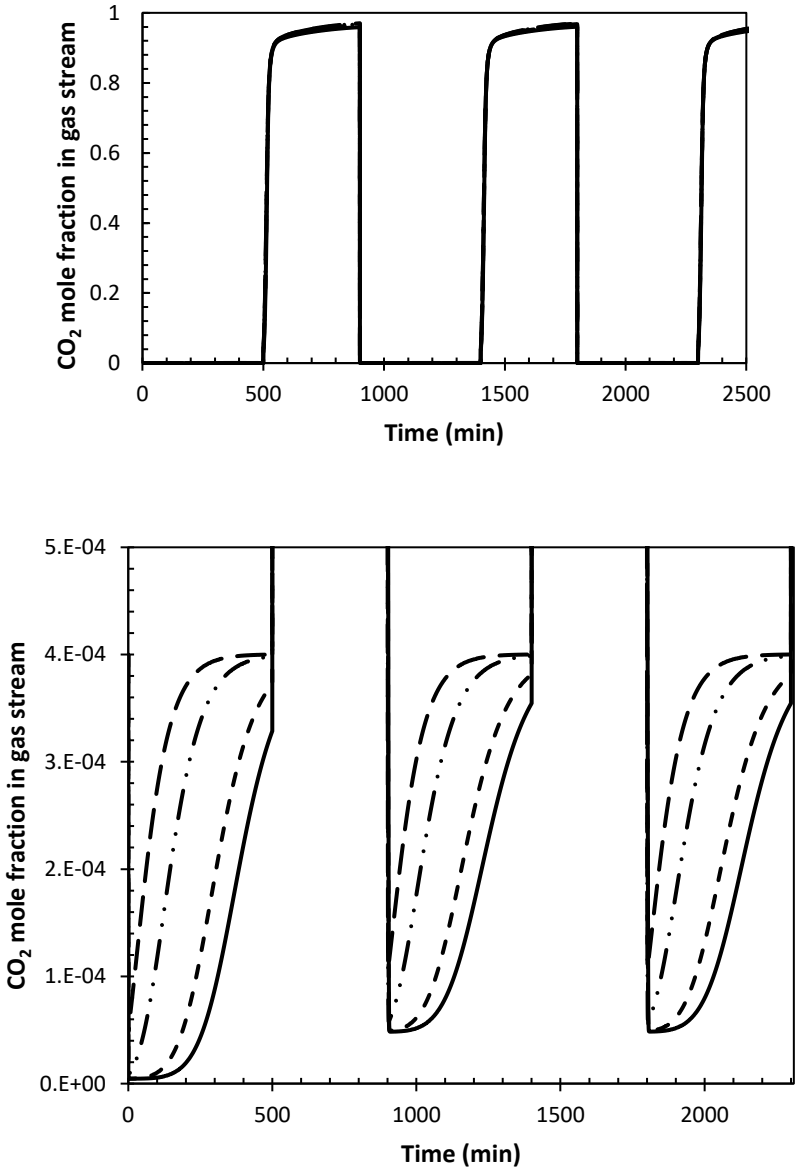


Figure 8. CO_2 uptake on (a) SIFSIX-3-Cu and (b) Mg-MOF-74 at various locations along the bed. The simulation conditions involved an operating pressure of 1.25 bar, temperature of 298 K, CO_2 concentration of 400 ppm in N_2, and a feed flow rate of 20 mL min^{-1}.

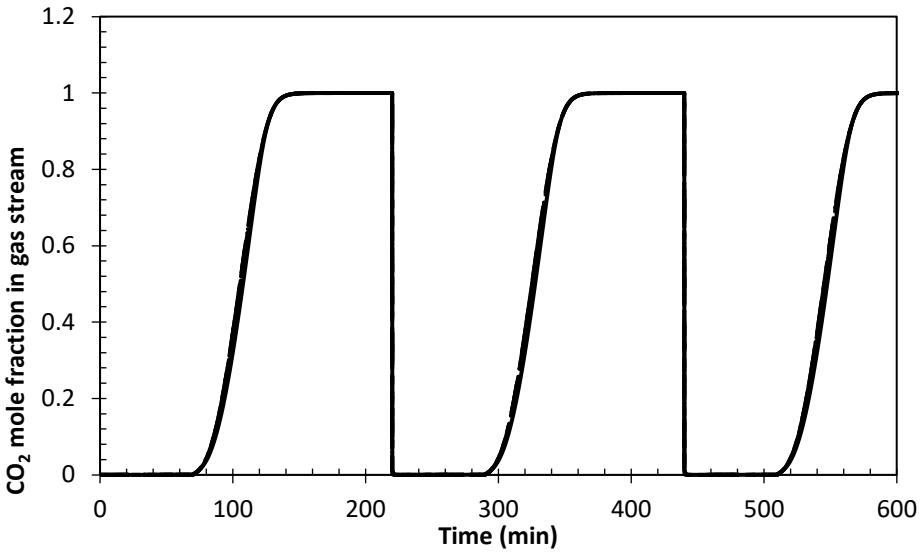
3.3.3 Cycles of adsorption; desorption by pure CO_2 stream

Here, we study the cyclic process of adsorption and desorption. The desorption steps involve the use of a CO_2 at 398 K. Figs. 9 and 10 display CO_2 mole fraction within the gas phase during consecutive cycles of adsorption and desorption. It is evident that the molar fraction of CO_2 in the gas phase during the desorption steps approaches unity, thereby indicating that the adsorbents demonstrate limited adsorption of N_2 while primarily adsorbing CO_2. Hence, a significant amount of CO_2 is generated during the desorption phase, resulting in elevated concentrations. The generation of a substantial quantity of CO_2 offers a significant benefit, as it renders CO_2 more amenable for integration into various additional processes, such as enhanced oil recovery[46]. The generation of elevated concentrations of CO_2 indeed stands as a pivotal element in appraising the efficacy of process performance.

Considering that the molar fraction of CO_2 in the gas phase in the adsorption phase is about 400 ppm, therefore, it is not clear in the curves. To enhance lucidity, a segment of the curves is presented in fractional moles, ensuring the complete elucidation of CO_2 variations.



Figures 9. Cyclic breakthrough curves for CO_2 adsorption on SIFSIX-3-Cu. The adsorption process occurred at 1.25 bar, 298 K, with a CO_2 concentration of 400 ppm in N_2 and a feed flow rate of 20 mL min^{-1}. The subsequent desorption step involved the flow of pure CO_2 at 0.01 bar and 398 K.


1.2
1
0.8
0.6
0.4
0.2
0
CO_2 mole fraction in gas stream
0
100
200
300
400
500
600
Time (min)

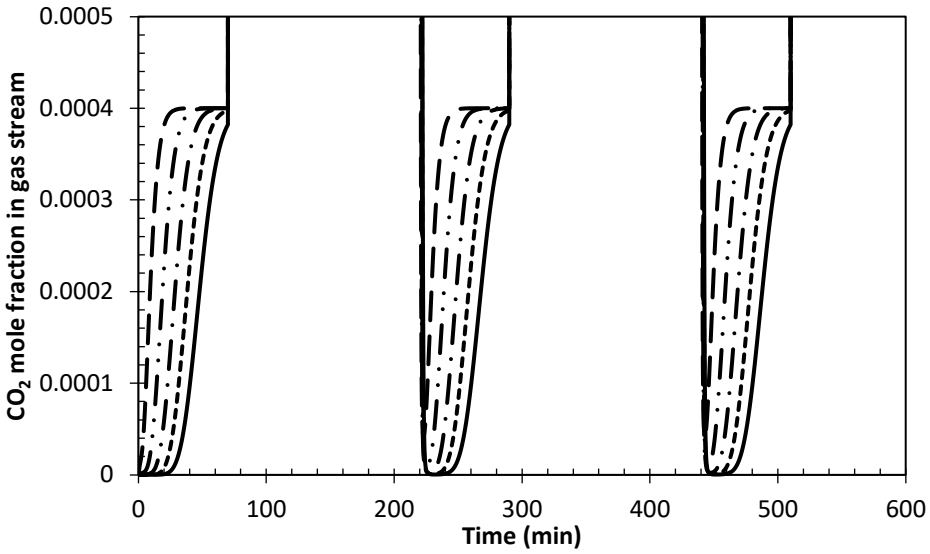


Figure 10. Cyclic breakthrough curves for CO_2 adsorption on Mg-MOF-74. The adsorption process occurred at 1.25 bar, 298 K, with a CO_2 concentration of 400 ppm in N_2 and a feed flow rate of 20 mL min^{-1}. The subsequent desorption step involves the flow of pure CO_2 at 0.01 bar and 398 K.

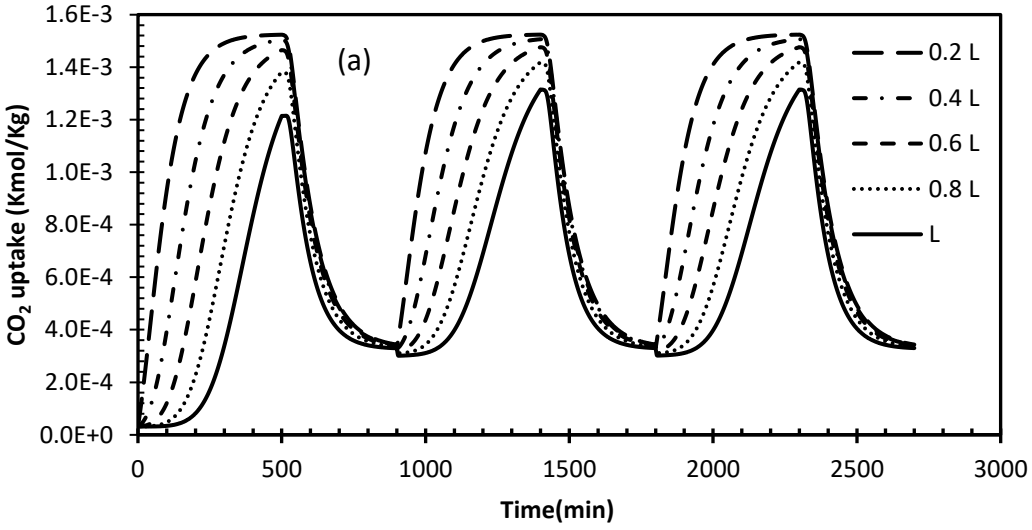
3.3.3 Cycles of adsorption; desorption by heat jacket

The desorption stage assumes a pivotal role in gas separation by solid adsorbents. Effectively adjusting the desorption conditions can yield substantial effects in various facets of the process, such as energy efficiency, adsorbent longevity, and CO_2 purity. The necessity to maintain temperature stability of the solid adsorbent in desorption stage emerges as a crucial aspect in the effectiveness of the desorption stage, owing to the demand for higher temperatures compared to the adsorption process. The rationale behind this is attributed to the need for energy to be inputted into the system for the process of desorption. The desorption stage commonly occurs under reduced pressure in contrast to the adsorption process. In the DAC process, which takes place at standard atmospheric pressure, the desorption pressure generally falls below the ambient pressure, thereby inducing a state of relative vacuum. The optimization of the desorption pressure is of paramount importance when considering the economic aspects of the process.

To achieve the stated objective, Fig. 11 illustrates the CO_2 adsorption behavior of SIFSIX-3-Cu and Mg-MOF-74 sorbents. The desorption step is carried out at a 398 K and 0.01 kPa. Thermal insulation and heat retention are ensured by employing a thermal jacket around the column. The

obtained data indicates that the CO_2 uptakes on SIFSIX-3-Cu and Mg-MOF-74 are 1.5 and 0.12 mmol/g, respectively. During the desorption process, these values decrease to 0.0000333 and 0.0000051 mmol/g, respectively. SIFSIX-3-Cu exhibits a desorption efficiency of around 78% for CO_2, while Mg-MOF-74 demonstrates a CO_2 desorption capacity of 53%.

Figures S4 and S5 depict the observed CO_2 concentrations within the sorbent during the adsorption and desorption steps, specifically when the desorption temperature reaches 373 K. The results presented in Figures S4 and S5 clearly indicate a decrease in CO_2 desorption when subjected to temperatures below 398 K. At 373 K, SIFSIX-3-Cu exhibits a 51% CO_2 desorption, whereas Mg-MOF-74 demonstrates a 17% CO_2 release. It is important to note that although the pores of Mg-MOF-74 are larger than those of SIFSIX-3-Cu, the low amount of CO_2 adsorbed on the Mg-MOF-74 leads to a lower desorption percentage. Nonetheless, it can be argued that a desorption temperature of 398 K would be a more suitable choice.



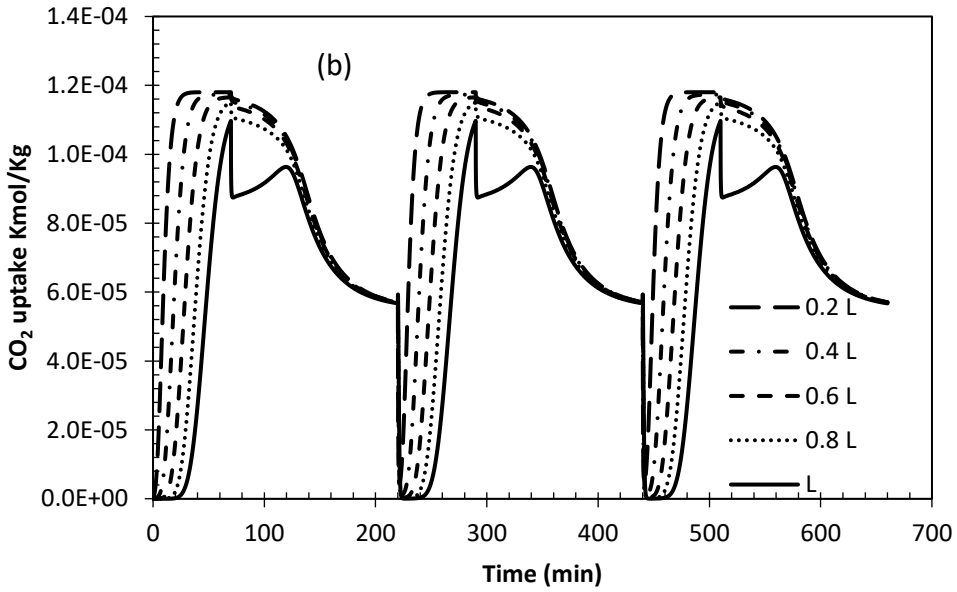


Figure 11. Cyclic CO_2 uptake curves for CO_2 adsorption on (a) SIFSIX-3-Cu and (b) Mg-MOF-74. The adsorption step was conducted at 1.25 bar, 298 K, with a CO_2 concentration of 400 ppm in N_2 and a feed flow rate of 20 mL min^{-1}. The desorption step was performed at 398 K and 0.01 bar using pure CO_2

Figure 12 exhibits the extent of CO_2 desorption from SIFSIX-3-Cu at two distinct desorption pressures 0.01 and 0.05 kPa. By elevating the desorption pressure from 0.01 to 0.05 kPa, a pronounced decline in desorption quantity and a consequential diminishment in the system's general efficiency can be observed. The noteworthy propensity of SIFSIX-3-Cu towards CO_2, including under low pressure conditions, is accountable for the susceptibility of the desorption process towards changes in pressure. The degree of sensitivity exhibited by the system can exert a pronounced influence on its overall efficiency.

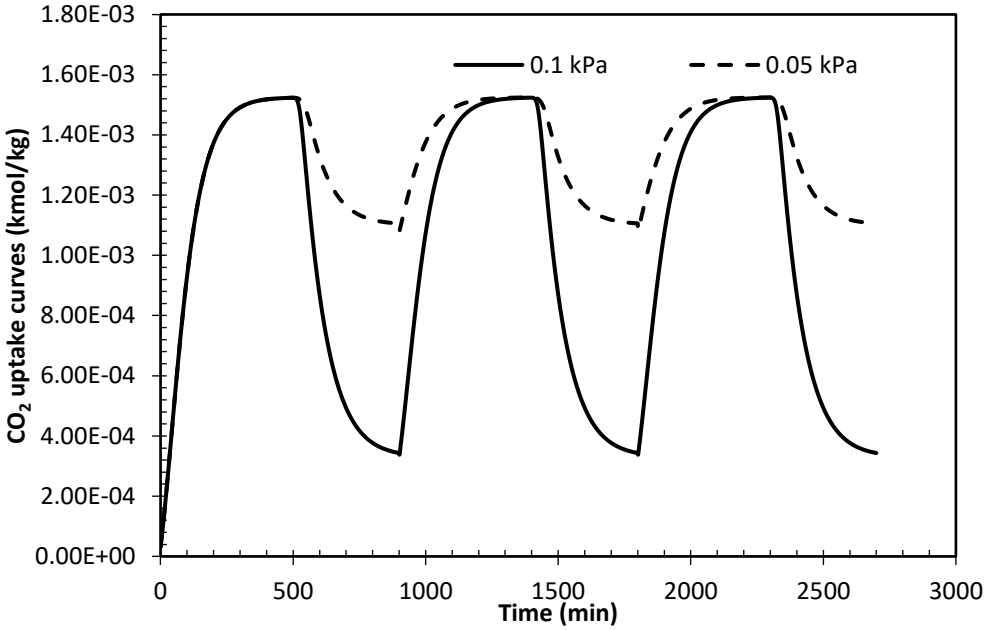
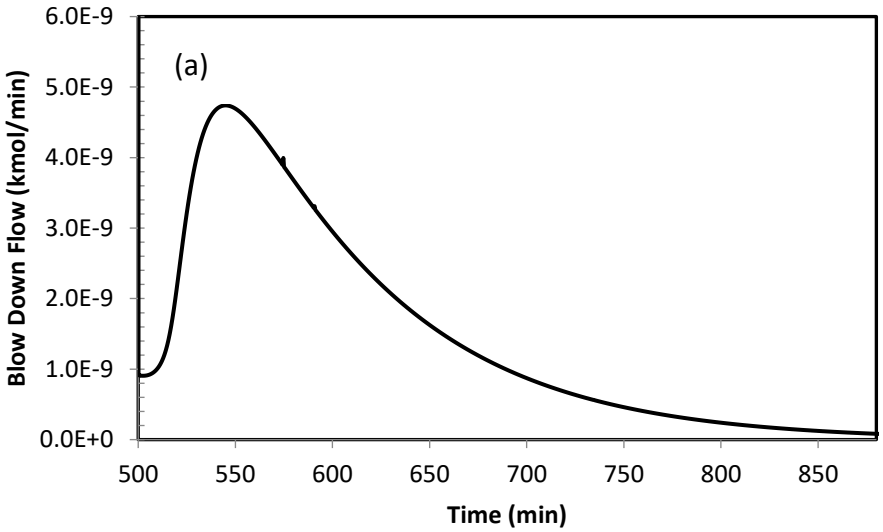


Figure 12. Cycle CO_2 uptake curves for the CO_2 adsorption on SIFSIX-3-Cu: Adsorption at 1.25 bar, 298 K, 400 ppm CO_2 in N_2, 20 mL min^{-1}; Desorption at 398 K and different pressures

Figure 13 depicts the blowdown flow rate observed during the desorption step in DAC for both SIFSIX-3-Cu and Mg-MOF-74 .Notably, the results indicate that the SIFSIX-3-Cu packed bed exhibits a superior CO_2 flow rate in comparison to Mg-MOF-74. The observed contrast is attributed to the augmented amount of CO_2 adsorbed on SIFSIX-3-Cu. Hence, the SIFSIX-3-Cu sorbent exhibits substantial potential in generating a significant quantity of enriched CO_2. A noteworthy characteristic of the SIFSIX-3-Cu structure is its small pores, enabling the release of CO_2 to occur in a single step during desorption. There is a slight delay before the release commences, reaching a peak and gradually decreasing thereafter. This process of CO_2 release occurs as the adsorber undergoes temperature elevation to achieve the regeneration temperature. In contrast, the Mg-MOF-74 sorbent releases CO_2 in two steps. Initially, a significant portion of the adsorbed CO_2 is released as the pressure decreases. Subsequently, in the second step, the remaining CO_2 is expelled as the temperature of the solid surface increases. Figure 14 illustrates the temperature fluctuations of the solids during the adsorption and desorption stages for both sorbents. Due to the continuous flow of the feed in the column, the heat of adsorption has minimal

impact on the temperature throughout the adsorption process, resulting in a consistent temperature trend for both sorbents. However, during the desorption steps, the trends diverge. This disparity arises because SIFSIX-3-Cu possesses narrow pores and exhibits a strong interaction with CO_2, necessitating low pressure and high temperature for the removal of CO_2 molecules from its structure. Therefore, despite the pressure reduction during the desorption step, the process remains incomplete until the adsorbent surface attains the desired temperature. Consequently, desorption occurs gradually. For Mg-MOF-74, the desorption step exhibits distinct characteristics. As the pressure decreases, a significant portion of the molecules is liberated due to the MOF's relatively larger pores, which facilitate the release. Moreover, the sudden decrease in solid temperature can be attributed to the heat generated during desorption. When subjected to thermal energy from the thermal jacket, the temperature of the adsorbent solid rises, causing the remaining CO_2 molecules to desorb. The desorption process in Mg-MOF-74 typically occurs in two steps, owing to the varying interaction strengths between CO_2 and the two adsorption sites present in the material. CO_2 desorption initially takes place from the weaker sites, followed by desorption from the stronger sites, as governed by the utilization of dual-site Langmuir adsorption isotherms for CO_2 adsorption.



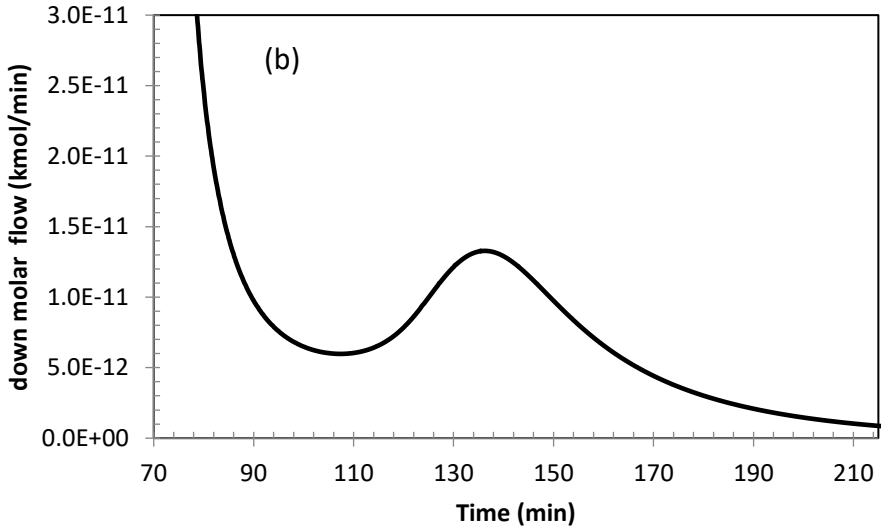


Figure 13. Blow down molar flow rate in desorption step for (a) SIFSIX-3-Cu and (b) Mg MOF-74. Adsorption at 1.25 bar, 298 K, 400 ppm CO_2 in N_2, 20 mL min^{-1}; Desorption at 0.01 bar, 398 K

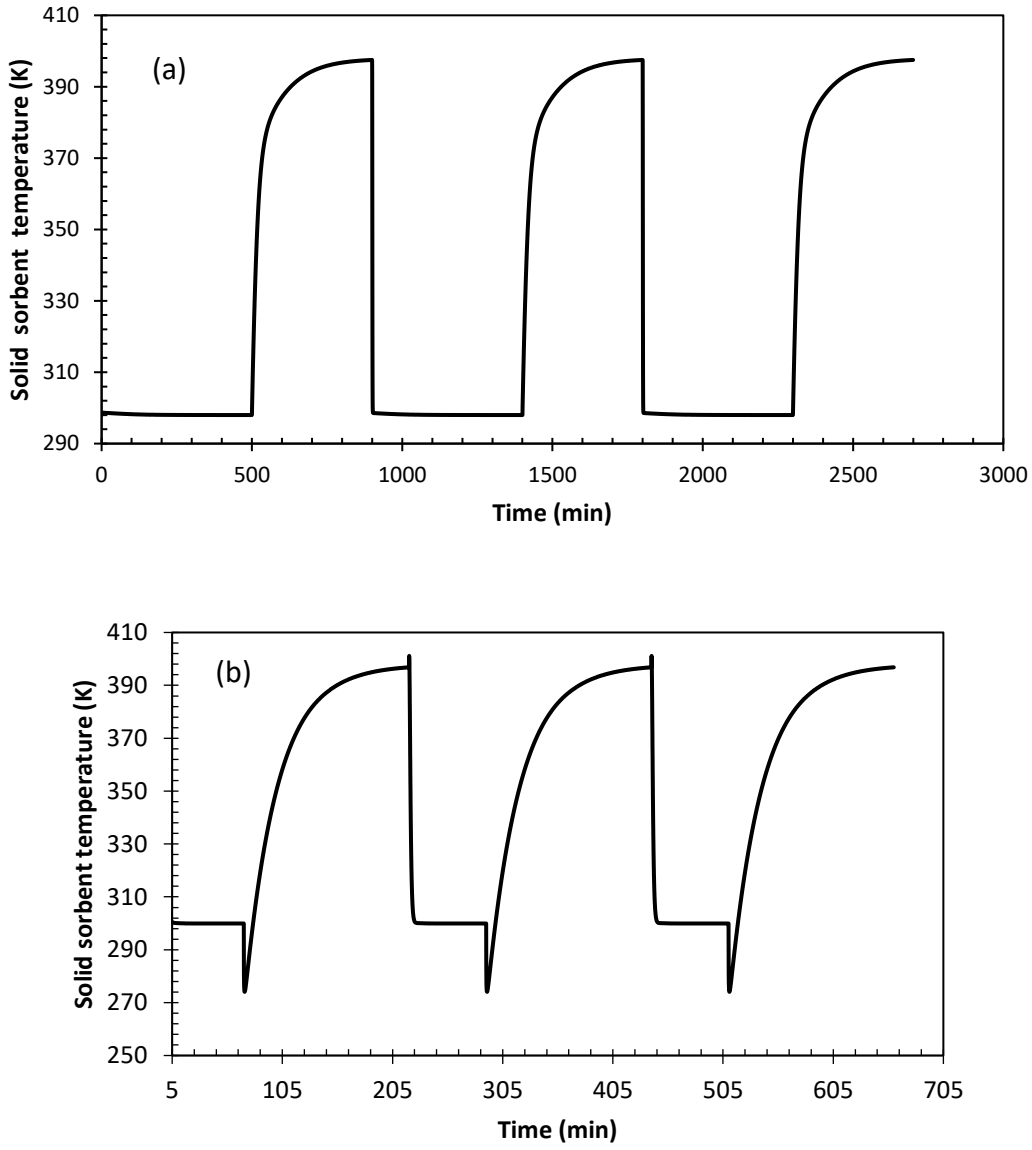


Figure 14. Temperature of (a) SIFSIX-3-Cu and (b) Mg-MOF-74 sorbent in column for adsorption at 1.25 bar, 298 K, 400 ppm CO_2 in N_2, 20 mL min^{-1}; Desorption at 0.01 bar, 398 K

4.1 Limitations and Future Work

While this study provides valuable insights into the performance of SIFSIX-3-Cu for direct air capture applications, several limitations should be acknowledged. The most significant limitation is the reliance on computational simulations without direct experimental validation of the packed bed performance. Although the GCMC simulations were benchmarked against literature data and demonstrated good agreement with experimental CO_2 adsorption isotherms, real packed bed systems may exhibit dynamic behaviors that are not fully captured by the current modeling

approach. Future research should aim to experimentally validate the computational findings by synthesizing and characterizing both SIFSIX-3-Cu and Mg-MOF-74, measuring pure and mixed-gas adsorption isotherms at various temperatures, and performing laboratory-scale breakthrough tests to confirm the predicted breakthrough times. Additionally, conducting cyclic adsorption-desorption experiments is crucial to evaluate the long-term stability of the materials. Measuring CO_2 adsorption kinetics under both trace (400 ppm) and high-concentration conditions would further strengthen the understanding of material behavior under DAC-relevant scenarios. Finally, the impact of humidity on CO_2 capture performance should be studied experimentally, as water vapor co-adsorption may significantly alter the efficiency and selectivity of the materials in realistic ambient conditions.

CONCLUSIONS

SIFSIX-3-Cu has strong CO_2 adsorption capacities even at 400 ppm concentrations, making it effective in capturing CO_2 from air. The simulation of packed bed columns shows SIFSIX-3-Cu performs better than Mg-MOF-74, with a breakthrough time of 500 minutes compared to 70 minutes. The temporal variation analysis highlights the higher CO_2 uptake of SIFSIX-3-Cu (1.4 mmol g^{-1}) under ambient conditions, compared to Mg-MOF-74 (0.12 mmol g^{-1}). This performance is due to the strong CO_2 adsorption of SIFSIX-3-Cu, thanks to its narrow pores and strong CO_2 interaction. Moreover, SIFSIX-3-Cu shows a gradual release of CO_2 during desorption, necessitating high temperature and low pressure for efficient desorption. Mg-MOF-74 releases CO_2 in two steps due to larger pores and heat generation during desorption. These findings highlight the potential of SIFSIX-3-Cu for DAC, especially in air CO_2 capture. The high CO_2 adsorption by SIFSIX-3-Cu, even at low concentrations, makes it perfect for carbon capture by DAC. Additionally, the study reveals that SIFSIX-3-Cu exhibits superior selectivity for CO_2 over N_2, which is crucial for efficient DAC operations in ambient air. To further enhance the performance and scalability of SIFSIX-3-Cu for DAC, it is recommended to investigate its long-term stability under continuous adsorption-desorption cycles, explore its integration with renewable energy sources to reduce energy requirements, and conduct pilot-scale studies to evaluate its performance in real-world DAC systems.

ACKNOWLEDGMENTS

We would like to appreciate the financial assistance of Memorial University, InnovateNL, Ilam University and the Research Council of Finland (Grant no. 346846). To improve the clarity and

fluency of the English writing, assistance from AI-based language tools was used during the manuscript preparation.

REFERENCES

[1] Keith DW. Why capture CO2 from the atmosphere? Science (80-) 2009;325:1654–5.

[2] Agrawala S. Context and early origins of the Intergovernmental Panel on Climate Change. Clim Change 1998;39:605–20.

[3] Herzog H. What future for carbon capture and sequestration? Environ Sci Technol 2001;35:148A.

[4] Ozkan M. Direct air capture of CO2: A response to meet the global climate targets. MRS Energy Sustain 2021;8:51–6.

[5] Ramasamy S, Basak PR, Patra SP. Capture and use CO2 with Carbon Clean Solutions (CCS). Int J Chem Synth Chem React 2018;4:5–10.

[6] Kumar A, Madden DG, Lusi M, Chen KJ, Daniels EA, Curtin T, et al. Direct air capture of CO2 by physisorbent materials. Angew Chemie Int Ed 2015;54:14372–7.

[7] Ochedi FO, Yu J, Yu H, Liu Y, Hussain A. Carbon dioxide capture using liquid absorption methods: a review. Environ Chem Lett 2021;19:77–109.

[8] Zhu X, Xie W, Wu J, Miao Y, Xiang C, Chen C, et al. Recent advances in direct air capture by adsorption. Chem Soc Rev 2022;51:6574–651.

[9] Findley JM, Sholl DS. Computational screening of MOFs and zeolites for direct air capture of carbon dioxide under humid conditions. J Phys Chem C 2021;125:24630–9.

[10] Leonzio G, Mwabonje O, Fennell PS, Shah N. Environmental performance of different sorbents used for direct air capture. Sustain Prod Consum 2022;32:101–11.

[11] Sadiq MM, Batten MP, Mulet X, Freeman C, Konstas K, Mardel JI, et al. A pilot scale demonstration of mobile direct air capture using metal organic frameworks. Adv Sustain Syst 2020;4:2000101.

[12] Qasem NAA, Ben-Mansour R. Adsorption breakthrough and cycling stability of carbon dioxide separation from CO2/N2/H2O mixture under ambient conditions using 13X and Mg-MOF-74. Appl Energy 2018;230:1093–107.

[13] Burns TD, Pai KN, Subraveti SG, Collins SP, Krykunov M, Rajendran A, et al. Prediction of MOF performance in vacuum swing adsorption systems for postcombustion CO2 capture based on integrated molecular simulations, process optimizations, and machine learning models. Environ Sci Technol 2020;54:4536–44.

[14] Wilson SMW, Tezel FH. Direct dry air capture of CO2 using VTSA with faujasite

zeolites. Ind Eng Chem Res 2020;59:8783–94.

[15] Liu W, Lin YC, Ji Y, Yong JY, Zhang XJ, Jiang L. Thermodynamic study on two adsorption working cycles for direct air capture. Appl Therm Eng 2022;214:118920.

[16] Dureckova H, Krykunov M, Aghaji MZ, Woo TK. Robust machine learning models for predicting high CO2 working capacity and CO2/H2 selectivity of gas adsorption in metal organic frameworks for precombustion carbon capture. J Phys Chem C 2019;123:4133–9.

[17] Xiao T, Liu D. The most advanced synthesis and a wide range of applications of MOF-74 and its derivatives. Microporous Mesoporous Mater 2019;283:88–103.

[18] Kumar A, Hua C, Madden DG, O□Nolan D, Chen K-J, Keane L-AJ, et al. Hybrid ultramicroporous materials (HUMs) with enhanced stability and trace carbon capture performance. Chem Commun 2017;53:5946–9.

[19] Custelcean R. Direct air capture of CO 2 via crystal engineering. Chem Sci 2021;12:12518–28.

[20] Shekhah O, Belmabkhout Y, Chen Z, Guillerm V, Cairns A, Adil K, et al. Made-to-order metal-organic frameworks for trace carbon dioxide removal and air capture. Nat Commun 2014;5:4228.

[21] Forrest KA, Pham T, Elsaidi SK, Mohamed MH, Thallapally PK, Zaworotko MJ, et al. Investigating CO2 sorption in SIFSIX-3-M (M= Fe, Co, Ni, Cu, Zn) through computational studies. Cryst Growth Des 2019;19:3732–43.

[22] Bayati B, Keshavarz F, Rezaei N, Zendehboudi S, Barbiellini B. New insight into impact of humidity on direct air capture performance by SIFSIX-3-Cu MOF. Phys Chem Chem Phys 2024;26:17645–59.

[23] Ben-Mansour R, Olufemi Eyitope B, Antar MA. Simulation of adsorptive storage of CO2 in fixed bed of MOF-5. J Energy Resour Technol 2016;138:12001.

[24] Elsaidi SK, Mohamed MH, Helal AS, Galanek M, Pham T, Suepaul S, et al. Radiation-resistant metal-organic framework enables efficient separation of krypton fission gas from spent nuclear fuel. Nat Commun 2020;11:3103.

[25] Ziaee A, Chovan D, Lusi M, Perry IV JJ, Zaworotko MJ, Tofail SAM. Theoretical optimization of pore size and chemistry in SIFSIX-3-M hybrid ultramicroporous materials. Cryst Growth Des 2016;16:3890–7.

[26] Cho Y, Teetz J, Kulik HJ. Assessing UFF and DFT-Tuned Force Fields for Predicting Experimental Isotherms of MOFs. J Chem Inf Model 2024.

[27] Barcia PS, Silva JAC, Rodrigues AE. Adsorption dynamics of C5- C6 isomerate fractions in zeolite beta for the octane improvement of gasoline. Energy & Fuels 2010;24:1931–40.

[28] Casas N, Schell J, Pini R, Mazzotti M. Fixed bed adsorption of CO 2/H 2 mixtures on activated carbon: experiments and modeling. Adsorption 2012;18:143–61.

[29] Khalkhali M, Ghorbani A, Bayati B. Study of adsorption and diffusion of methyl mercaptan and methane on FAU zeolite using molecular simulation. Polyhedron

2019;171:403–10.

[30] Roy S, Moharir AS. Modeling the generic breakthrough curve for adsorption process. ArXiv Prepr ArXiv190700195 2019.

[31] Ben-Mansour R, Qasem NAA. An efficient temperature swing adsorption (TSA) process for separating CO2 from CO2/N2 mixture using Mg-MOF-74. Energy Convers Manag 2018;156:10–24.

[32] Qiu H, Lv L, Pan B, Zhang Q, Zhang W, Zhang Q. Critical review in adsorption kinetic models. J Zhejiang Univ A 2009;10:716–24.

[33] McKay G, Allen SJ, McConvey IF, Walters JHR. External mass transfer and homogeneous solid-phase diffusion effects during the adsorption of dyestuffs. Ind Eng Chem Process Des Dev 1984;23:221–6.

[34] Magalh□es Siqueira R, Vilarrasa-Garc□a E, Belo Torres AE, Silva de Azevedo DC, Bastos-Neto M. Simple procedure to estimate mass transfer coefficients from uptake curves on activated carbons. Chem Eng Technol 2018;41:1622–30.

[35] Hu Z, Wang Y, Shah BB, Zhao D. CO2 capture in metal□organic framework adsorbents: an engineering perspective. Adv Sustain Syst 2019;3:1800080.

[36] Zhan G, Bai L, Wu B, Cao F, Duan Y, Chang F, et al. Dynamic process simulation and optimization of CO2 removal from confined space with pressure and temperature swing adsorption. Chem Eng J 2021;416:129104.

[37] Gutierrez-Ortega A, Montes-Mor□n MA, Parra JB, Sempere J, Nomen R, Gonzalez-Olmos R. Comparative study of binderless zeolites and carbon molecular sieves as adsorbents for CO2 capture processes. J CO2 Util 2022;61:102012.

[38] Da Silva FA, Silva JA, Rodrigues AE. A general package for the simulation of cyclic adsorption processes. Adsorption 1999;5:229–44.

[39] Adil K, Bhatt PM, Belmabkhout Y, Abtab SMT, Jiang H, Assen AH, et al. Valuing metal□organic frameworks for postcombustion carbon capture: a benchmark study for evaluating physical adsorbents. Adv Mater 2017;29:1702953.

[40] Yuan J, Liu X, Li X, Yu J. Computer simulations for the adsorption and separation of CH4/H2/CO2/N2 gases by hybrid ultramicroporous materials. Mater Today Commun 2021;26:101987.

[41] Malek A, Farooq S. Comparison of isotherm models for hydrocarbon adsorption on activated carbon. AIChE J 1996;42:3191–201.

[42] Nikolaidis GN, Kikkinides ES, Georgiadis MC. An integrated two-stage P/VSA process for postcombustion CO2 capture using combinations of adsorbents zeolite 13X and Mg-MOF-74. Ind Eng Chem Res 2017;56:974–88.

[43] Sircar S, Myers A. Gas Separation by Zeolites 2003. https://doi.org/10.1201/9780203911167.ch22.

[44] Alonso G, Bahamon D, Keshavarz F, Gim□nez X, Gamallo P, Sayo s R n. Density

functional theory-based adsorption isotherms for pure and flue gas mixtures on Mg-MOF-74. Application in CO2 capture swing adsorption processes. J Phys Chem C 2018;122:3945–57.

[45] Mason JA, Sumida K, Herm ZR, Krishna R, Long JR. Evaluating metal□organic frameworks for post-combustion carbon dioxide capture via temperature swing adsorption. Energy Environ Sci 2011;4:3030–40.

[46] Farajzadeh R, Eftekhari AA, Dafnomilis G, Lake LW, Bruining J. On the sustainability of CO2 storage through CO2□Enhanced oil recovery. Appl Energy 2020;261:114467.

Supplementary Files

This is a list of supplementary files associated with this preprint. Click to download.

- Supplementary.docx